Images of bottomside irregularities observed at topside altitudes

William J. Burke,[1,2] Louise C. Gentile,[1] Shannon R. Shomo,[1] Patrick A. Roddy,[1] and Robert F. Pfaff[3]

Received 16 September 2011; revised 16 December 2011; accepted 9 January 2012; published 29 March 2012.

[1] We analyzed plasma and field measurements acquired by the Communication/Navigation Outage Forecasting System (C/NOFS) satellite during an eight-hour period on 13–14 January 2010 when strong to moderate 250 MHz scintillation activity was observed at nearby Scintillation Network Decision Aid (SCINDA) ground stations. C/NOFS consistently detected relatively small-scale density and electric field irregularities embedded within large-scale (∼100 km) structures at topside altitudes. Significant spectral power measured at the Fresnel (∼1 km) scale size suggests that C/NOFS was magnetically conjugate to bottomside irregularities similar to those directly responsible for the observed scintillations. Simultaneous ion drift and plasma density measurements indicate three distinct types of large-scale irregularities: (1) upward moving depletions, (2) downward moving depletions, and (3) upward moving density enhancements. The first type has the characteristics of equatorial plasma bubbles; the second and third do not. The data suggest that both downward moving depletions and upward moving density enhancements and the embedded small-scale irregularities may be regarded as Alfvénic images of bottomside irregularities. This interpretation is consistent with predictions of previously reported theoretical modeling and with satellite observations of upward-directed Poynting flux in the low-latitude ionosphere.

Citation: Burke, W. J., L. C. Gentile, S. R. Shomo, P. A. Roddy, and R. F. Pfaff (2012), Images of bottomside irregularities observed at topside altitudes, *J. Geophys. Res.*, *117*, A03332, doi:10.1029/2011JA017169.

1. Introduction

[2] The Communication/Navigation Outage Forecasting System (C/NOFS) mission was designed to specify and predict geophysical conditions that degrade the transionospheric propagation of radio signals at low latitudes. Its two major constituents are the C/NOFS satellite [*de La Beaujardière et al.*, 2004] and the Scintillation Network Decision Aid (SCINDA) global network of ground stations that monitor the quality of UHF and L band transmissions through the low-latitude ionosphere [*Groves et al.*, 1997]. The C/NOFS satellite is a three-axis stabilized vehicle that was launched in April 2008 into a 13° inclined orbit with initial apogee and perigee near 850 and 400 km, respectively. The satellite was a long time in the making; more than a full solar cycle passed between mission approval and launch. To prepare for the mission, a group of Air Force Research Laboratory (AFRL) analysts examined the systematics of equatorial plasma bubbles (EPBs) encountered in the evening local time sector by spacecraft of the Defense Meteorological Satellite Program (DMSP) [*Huang et al.*, 2001, 2002; *Gentile et al.*, 2006]. Subsequently, AFRL scientists associated with the ground-based part of the C/NOFS mission pointed out that scintillations of UHF signals were often observed at SCINDA sites during DMSP overflights when no EPB activity was detected. To reconcile these dissimilar ground- and space-based observations, *Burke et al.* [2003] compared 250 MHz scintillation activity observed at Ancon with 50 MHz coherent radar backscatter measured by the nearby Jicamarca unattended long-term studies of the ionosphere and atmosphere (JULIA) radar and with plasma densities measured during simultaneous DMSP overpasses. JULIA observations were divided into three classes: (1) an undisturbed ionosphere that yielded no scintillations, (2) plasma density irregularities confined to the bottomside layer, and (3) plumes of irregularities that extended well above the peak of the *F* layer. UHF scintillations were observed while JULIA detected signatures of the second and third types. Transitions between purely bottomside irregularities and topside plume signatures occurred when the S4 index for 250 MHz signals at Ancon exceeded 0.8. The S4 index is defined as the ratio of the standard deviation of signal amplitudes at a given carrier frequency to their mean value. During overflights, when JULIA detected plumes, DMSP detected EPBs in all but one instance. In that case, DMSP flew over the west coast of South America before the plume ascended to 840 km.

[3] When C/NOFS plasma measurements first became available, results of DMSP studies based on solar maximum conditions appeared moot. While EPBs were clearly an

[1]Air Force Research Laboratory Space Vehicles Directorate, Hanscom AFB, Massachusetts, USA.
[2]Boston College Institute for Scientific Research, Chestnut Hill, Massachusetts, USA.
[3]NASA Goddard Space Flight Center, Greenbelt, Maryland, USA.

Copyright 2012 by the American Geophysical Union.
0148-0227/12/2011JA017169

evening sector phenomenon during solar maximum and the previous solar minimum [*Huang et al.*, 2002], neither C/NOFS nor DMSP spacecraft encountered them at these local times during the late spring of 2008 [*Gentile et al.*, 2011]. Clear EPB signatures found in C/NOFS data streams appeared near or after local midnight [*Burke et al.*, 2009]. *De La Beaujardière et al.* [2009] identified a new class of deep plasma depletions in solar minimum that form after local midnight and persist through the dawn meridian. Plasma density measurements from C/NOFS and DMSP showed that these depletions can extend for several tens of degrees in both latitude and longitude [*Gentile et al.*, 2011]. The absence of EPBs at evening local times appears to be consistent with vector electric field measurements from C/NOFS. *Pfaff et al.* [2010] showed that signatures of prereversal enhancements [*Farley et al.*, 1986; *Fejer and Scherliess*, 1995], commonly regarded as crucial for EPB formation, were absent during this solar minimum. Still, UHF receivers at SCINDA stations continued to detect scintillation activity at evening local times. *Roddy et al.* [2010] compared plasma densities measured at C/NOFS altitudes with both scintillation and coherent backscatter data acquired at the Christmas Island SCINDA site (3°N, 157°W) from May 2008 to June 2009. They found that if the apex altitudes of field lines along the Christmas Island meridian were <600 km, the satellite encountered small-scale plasma density irregularities at topside altitudes while scintillations of 250 MHz signals were detected at ground level.

[4] It is widely accepted that radio wave scintillations represent effects of constructive and destructive interference patterns passing over the receiver. *Rufenach* [1975] attributed this interference pattern to wavefronts passing though a random phase screen region in the ionosphere above the receiver. Plasma density irregularities that accumulate on the bottomside of the *F* layer peak constitute the phase screen. To produce strong interference patterns on the ground, it is necessary that significant density irregularities be present in the ionospheric phase screen at or near the Fresnel scale [*Rufenach*, 1975] defined $F_S = \sqrt{2h\lambda}$. Here h is the altitude of the phase screen, which we approximate as the height of the F_2 peak density (h_MF_2); λ is the signal's free space wavelength. Calculations using the physics-based model (PBMOD) of the ionosphere [*Retterer et al.*, 2005] indicate that near the times and locations of present interest h_MF_2 ranged between 350 and 375 km. Thus, sensors on the satellite could only sample plasma and field parameters at topside altitudes. Since the free-space wavelength of a 250 MHz signal is 1.2 m, F_S ranged between 916 and 948 m. For simplicity in making comparisons with power spectral densities inferred from the C/NOFS plasma density and electric field measurements, we approximate the scale size of F_S as ~1 km.

[5] Scintillations of radio signals passing through the low-latitude ionosphere are caused by plasma density irregularities that grow at bottomside altitudes in the postsunset ionosphere via the Rayleigh-Taylor (R-T) instability. The R-T instability is usually regarded as a purely electrostatic ($\nabla \times \mathbf{E} = 0$) mode. *Basu* [2005] questioned the universality of this assumption and rederived the linear dispersion relation for R-T modes, keeping both Ampere's and Faraday's laws in his formulation. His analysis indicated that in the ionosphere, R-T modes have shear Alfvén wave components. Magnetic diffusion effectively damps the electromagnetic component of short-wavelength R-T modes. *Basu* [2005] concluded that for most computational purposes, the electrostatic approximation is justified. Scattered evidence of electromagnetic components for nonlinear R-T disturbances at long wavelengths has appeared in reported satellite measurements. The Dynamics Explorer-2 (DE-2) satellite encountered a large-amplitude Alfvén wave propagating along the upper boundary of an EPB that was moving upward at supersonic speed [*Aggson et al.*, 1992]. Subsequently, *Bhattacharyya and Burke* [2000] developed a transmission line model that predicted that Poynting flux should be observed propagating away from the magnetic equator under circumstances similar to those encountered by DE-2. Recently, evidence for the presence of Alfvénic perturbations near EPB boundaries has been found in measurements from the polar-orbiting Detection of Electro-Magnetic Emissions Transmitted from Earthquake Regions (DEMETER) [*Pottelette et al.*, 2007] and Challenging Minisatellite Payload (CHAMP) [*Park et al.*, 2008; *Stolle et al.*, 2006] satellites. Alfvénic and diamagnetic fluctuations are easily distinguishable in magnetic field measurements. The polarities of magnetic perturbations $\delta\mathbf{B}$ are normal to the main field $\mathbf{B}_0$ in the Alfvénic cases and along it in the diamagnetic. Germane to the present study, *Stolle et al.* [2006] reported measuring Poynting flux propagating away from the ionospheric footprints of some EPBs as well as from the equatorial field-line apex of others. However, to date, no one has reported detecting magnetic perturbations with ~1 km scale sizes.

[6] The purpose of this case study is to re-examine evening sector plasma and field measurements acquired at topside altitudes by sensors on the C/NOFS satellite while strong scintillations of UHF signals were being observed at three SCINDA stations. Section 2 describes relevant C/NOFS sensor capabilities. Section 3 concentrates on high-resolution variations in plasma density and drifts as well as on attendant electric and magnetic field measurements acquired during the three overpasses of the Cape Verde (16.7°N, 337.1°E), São Luis (2.6°S, 315.8°E), and Ancon (11.8°S, 282.9°E) SCINDA stations on the UT night of 13–14 January 2010 when scintillations of 250 MHz signals were observed. Plasma density and drift measurements indicate the presence of local depletions and enhancements at topside altitudes with scale sizes of ~100 km that moved either upward or downward with respect to plasma on nearby flux tubes. Sensors on C/NOFS consistently sampled small-scale, broadband density, electric and occasionally magnetic field fluctuations embedded in ~100 km scale disturbances. In section 4, we suggest that in addition to EPBs, C/NOFS encountered purely topside disturbances that were magnetically conjugate to growing R-T density irregularities still confined to bottomside altitudes. We suggest that the conjugate irregularities were most likely formed and maintained via a broadband spectrum of Alfvén waves propagating in the affected flux tubes.

2. Instrumentation

[7] The three sensors on the C/NOFS satellite whose measurements are used in this paper are the Planar Langmuir

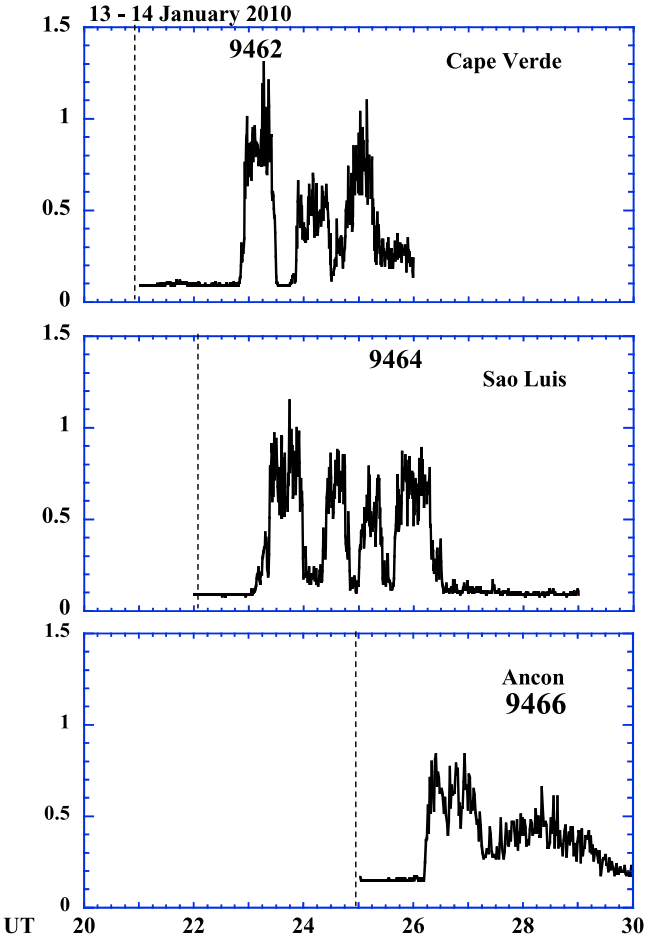

Figure 1. S4 index for 250 MHz signals observed at (top) Cape Verde, (middle) São Luis and (bottom) Ancon on the night of 13–14 January 2010. Vertical dashed lines mark approximate times that the ionosphere above these SCINDA stations passed into darkness. Approximate times of C/NOFS overpasses are indicated by orbit numbers.

Probe (PLP), the Coupled Ion Neutral Dynamics Investigation (CINDI), and the Vector Electric Field Instrument (VEFI). This study relies primarily on data collected by the ion trap (IT) portion of the PLP. The IT is a grounded electrode mounted beneath three 80% transmission grids. The outermost grid is held at or near spacecraft ground. The second grid is normally held at −5 V to allow passage of all ions to the collection plate. The third grid is held at −12 V to prevent access of ambient electrons and to suppress photoelectron currents. The IT current is sampled at 2 kHz, passed through anti-alias filters then averaged to 512 Hz. Ion densities presented here are displayed as 1 min and 1 s averages. Currents sampled at 512 Hz are also used to calculate ion-density power spectra.

[8] As described on the CINDI Web site (http://cindispace.utdallas.edu/), CINDI has two major components that monitor neutral winds and plasma dynamics. The latter portion consists of an ion velocity meter (IVM) to measure the vertical (V_Z) and horizontal (V_H) cross-track components of the plasma velocity vector and a retarding potential analyzer to measure the ion densities (n_i), temperatures (T_i), and their in-track component of plasma velocity (V_X). Each parameter is reported at one-half second intervals. Here we only make use of V_Z and n_i measurements.

[9] VEFI consists of a central electronics package that receives input from three orthogonal pairs of 20 m tip-to-tip double probes and a fluxgate magnetometer on a 0.6 m boom [*Pfaff et al.*, 2010]. Vector electric fields are obtained with 16-bit words from potential differences measured between opposing collectors. Electric fields induced by the spacecraft motion are determined using magnetometer outputs. AC electric fields are measured by passing VEFI data streams though low (0–6 Hz) and high-pass (3–8,000 Hz) filters. AC magnetic field measurements with amplitudes between +/−900 nT are available in the 0–6 Hz band. Experience urges caution when interpreting AC magnetic field data acquired within deep density depletions. Oscillations induced in sensor preamplifiers can mask or obscure environmental signals.

3. Observations

[10] This paper focuses on ground and satellite measurements acquired between 20:00 UT on 13 January and 06:00 UT on 14 January 2010. Prevailing geomagnetic conditions were quiet, with $Dst = -9 \pm 3$ nT. Figure 1 shows traces of S4 indices plotted as functions of universal time (UT) for 250 MHz beacon signals monitored at the Cape Verde Islands (Figure 1, top), São Luis, Brazil (Figure 1, middle) and Ancon, Peru (Figure 1, bottom) stations. Vertical dashed lines mark approximate times when the ionosphere above these stations passed into darkness. Three C/NOFS orbit numbers are positioned to indicate the approximate intervals when the spacecraft passed from west to east near the SCINDA sites. Plasma and field measurements acquired during these orbits are examined in detail below. Data plotted in Figure 1 show that significant (S4 > 0.5) scintillations began at each station within 2 hours after sunset and ended near local midnight. The staccato nature of the observed enhanced S4 episodes and the wide longitudinal separations between stations suggest that local sequences of intermittent irregularities passed across the line of sight of the SCINDA stations. Differing S4 amplitudes indicate that the intensities of F_S irregularities must have also varied.

[11] Figure 2 (top) shows plasma densities measured by the PLP during C/NOFS orbit 9462 and the spacecraft altitude. Densities are presented as 1 min (black line) and 1 s (green line) averages. Outside the region highlighted by the red oval, the traces are nearly indistinguishable. The heavy dashed-line segment of the altitude trace (blue) marks the time when the spacecraft was in darkness. The spectrogram in Figure 2 (middle) shows the log of the power spectral densities (PSDs) accumulated over 3 s intervals starting at umbra entry and continuing until 10 min after exiting the Earth's shadow. Figure 2 (bottom) shows the C/NOFS orbit (red line) superposed onto a latitude-versus-local time grid, centered on local midnight. The green line marking the magnetic equator indicates that during this orbit C/NOFS stayed at low magnetic latitudes while crossing the Atlantic sector. Locations of the São Luis and Cape Verde stations are indicated by stars. In this type of display, local midnight is at the center of the figures and the orbits begin and end at consecutive ascending nodes. Consequently, data displays appear discontinuous when considered as functions of UT.

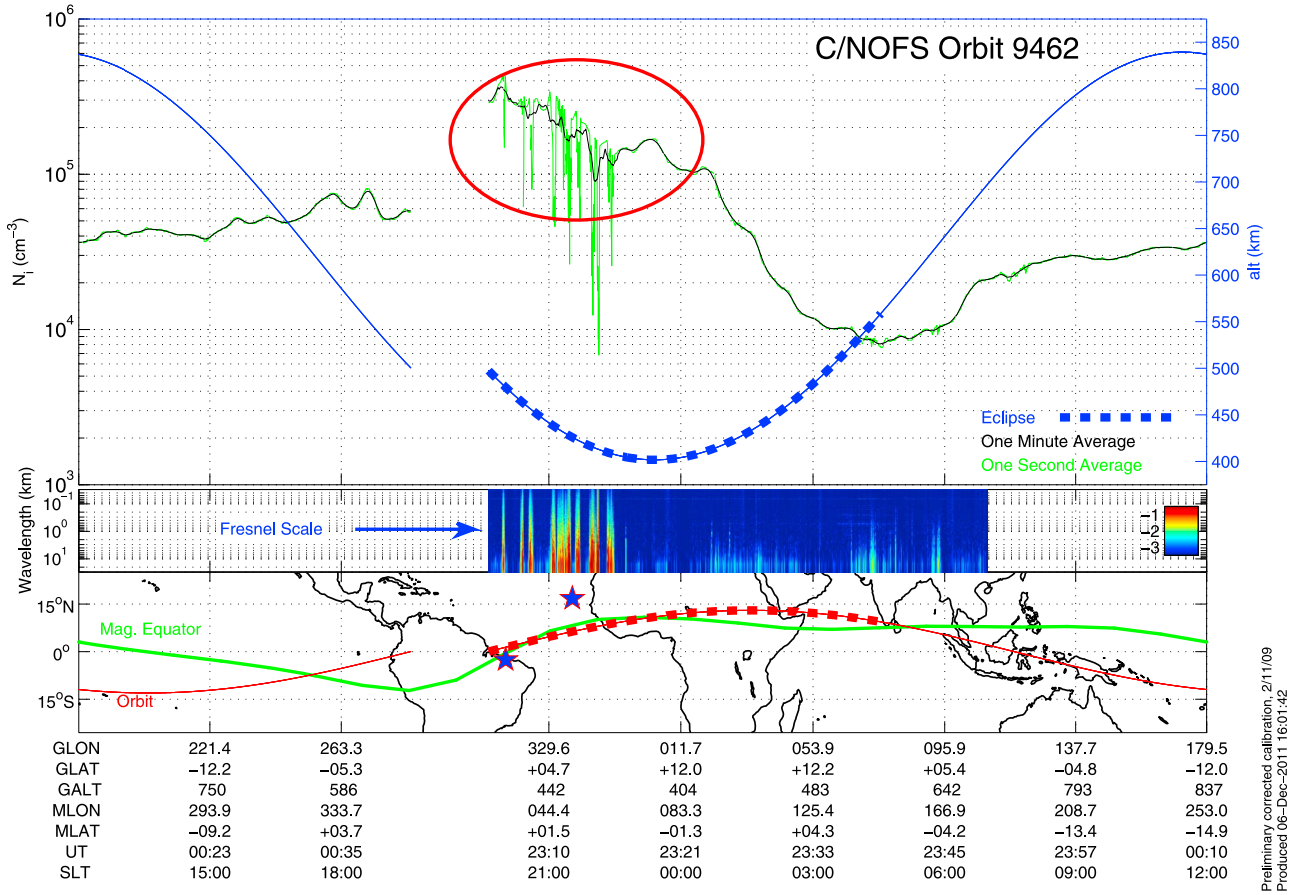

Figure 2. Measured plasma densities and orbital characteristics during C/NOFS orbit 9462. (top) Traces show densities measured at 1 min (black) and 1 s (green) resolution and spacecraft altitude (blue). (middle) The spectrogram indicates power at scale sizes between 10 and 0.01 km. (bottom) The map shows a projection of the C/NOFS orbit onto a latitude-versus-longitude grid, centered at local midnight. The green line marks the magnetic equator. Heavy dashed lines along the altitude and orbital traces indicate times when the spacecraft was in darkness.

Significant irregularity power is seen in the PSD spectrogram and the deep, localized depletions spanning the Atlantic sector from Brazil to West Africa.

[12] Figure 3 shows traces of plasma densities (dashed line) and the vertical component of drift (solid line) measured at half-second resolution by CINDI during the 12 min interval when C/NOFS was crossing the Atlantic Ocean. All of the depletions are characterized by upward plasma drifts. This is a classic signature of EPBs, that is, bottomside plasma that has ascended though the peak of the *F* layer to nominally topside altitudes. Figure 4a shows PLP density measurements acquired at 1 s resolution during the same 12 min interval. The trace is marked by a sequence of local depletions that typically took C/NOFS between 10 and 20 s

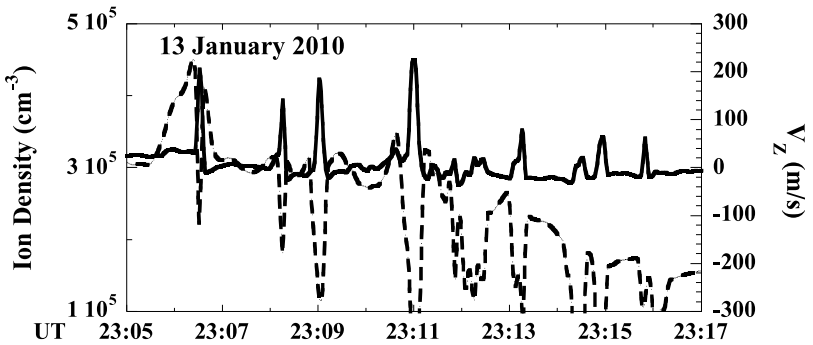

Figure 3. Ion densities (dashed line) and the vertical component of drift (solid line) measured by CINDI as C/NOFS crossed a region of irregularities during orbit 9462.

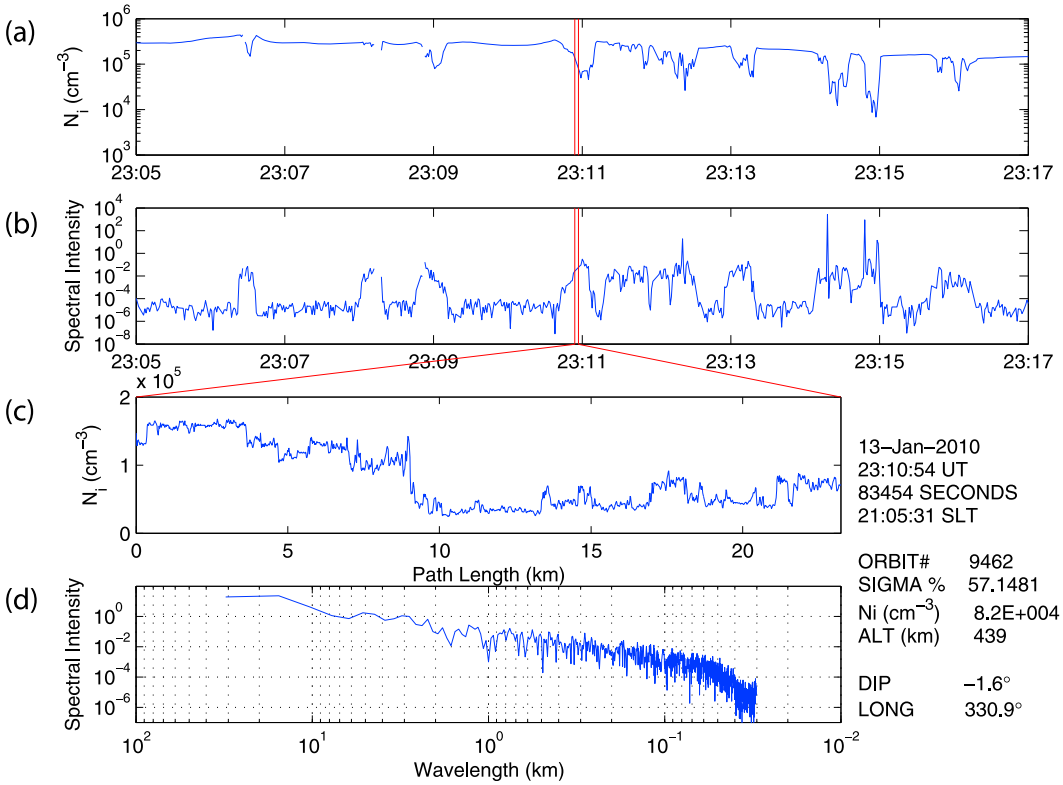

Figure 4. Plasma densities and power spectral characteristics sampled during C/NOFS orbit 9462 late on 13 January 2010. (a) The trace shows densities acquired over a 12 min period and displayed at 1 s resolution. (b) The spectral power at the Fresnel scale across the entire 12 min. (c) Ion densities sampled 512 times per second during the 3 s interval between the two vertical red lines. (d) The power spectral density calculated for this interval as a function of time.

to cross. For convenience, we refer to these as "large-scale" structures that have east-west dimensions of ~100 km. The two vertical lines along the western edge of the depletion crossed near 23:11 UT span 3 s. Figure 4b shows density-irregularity power at 1 km sampled over the same 12 min interval. We note that all the ~100 km scale depletions are marked by enhanced power at the Fresnel scale. Figures 4c and 4d provide a more detailed view of measurements within the 3 s interval marked by the red vertical lines. Densities sampled at a rate of 512 s^{-1} are shown in Figure 4c as a function of satellite path length. Figure 4d shows the power spectrum of $\delta N/N$ during the interval as a function of wavelength. $\delta N/N$ is calculated by dividing the difference between N and a linear fit to N by the linear fit to N. The power spectrum is derived by multiplying the Fourier transform of $\delta N/N$ by its complex conjugate, dividing the product by the sample size; this power is then normalized by the variance of $\delta N/N$. This power spectrum is dimensionless. Note that the power present at the approximate Fresnel scale within the density depletions is five orders of magnitude larger than in the surrounding undisturbed regions. This elevated power is considered significant. The spectrogram in the second panel of Figure 2 is a compilation of all PSDs accumulated while C/NOFS was in darkness during this orbit. For completeness, Figure 5 shows examples of high-pass PSDs derived from measurements by two electric field booms and the plasma density monitor on VEFI. Here the PSDs are given as functions of frequency rather than wavelength. Assuming a spacecraft speed of 7.5 km s^{-1}, a Fresnel scale of 1 km corresponds to a frequency of ~8 Hz. Thus, both the VEFI electric field and density measurements indicate significant power near the Fresnel scale.

[13] Information contained in Figure 6 was collected during C/NOFS orbit 9464 and is presented in the same format as Figure 2. Note that while the C/NOFS orbit was near the magnetic equator during the Cape Verde overpass, it was ~12° to the north of it during the nearest approach to São Luis. The trace in Figure 6 (top) shows that C/NOFS again crossed plasma depletions in the longitude sector from Brazil through West Africa. In agreement with S4 traces near 02:00 UT presented in Figure 1, the PSD spectrogram (Figure 6, middle) indicates that irregularities encountered near the longitude of São Luis UT were stronger than those measured near Cape Verde at ~02:40 UT). CINDI measurements (Figure 7) show a general upward motion of the ionosphere between 02:32 and 02:40 UT. However, in the depletions encountered while passing near the São Luis meridian (20:35 to 02:36 UT), plasma was moving downward relative to that in adjacent flux tubes to the east and west. In the previous example (Figure 3), all depletions moved in the upward direction. High-resolution PLP data shown in Figure 8 are presented in the same format as Figure 4. The 3 s data segment chosen to illustrate irregularities was acquired as C/NOFS crossed the eastern wall of

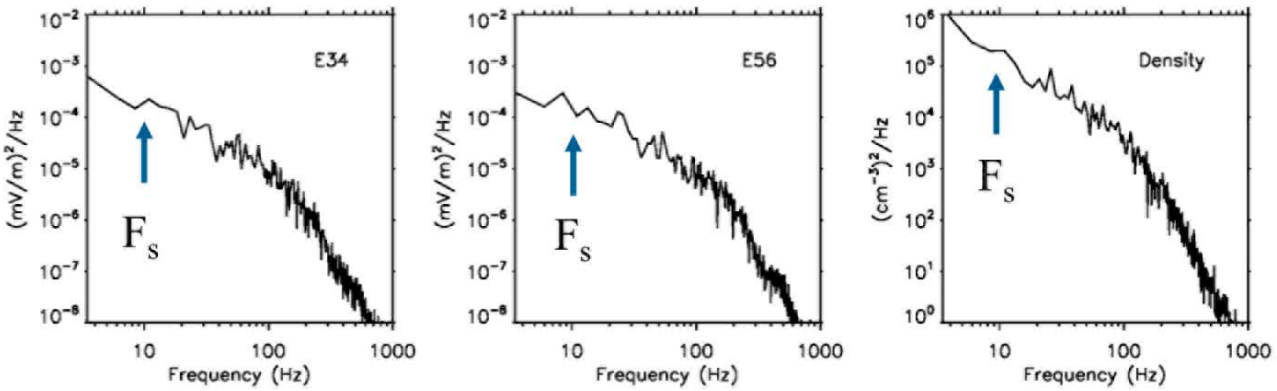

Figure 5. Examples of power spectral densities from VEFI between 3 and 1,000 Hz measured in (left and center) two components of the ambient electric field and (right) plasma density. Data used to calculate PSDs were acquired in a 2.015 s period starting at 23:11:15.642 UT on 13 January 2010.

the depletion near São Luis. Note that while significant spectral power was present at scale sizes near 1 km, its intensity was reduced by about two orders of magnitude in comparison with the example of Figure 4. The trace of spectral power near the Fresnel scale, found in Figure 8b, again shows local intensifications as C/NOFS crossed wider-scale depletions.

[14] Data acquired during C/NOFS orbit 9466, our final example, are shown in Figures 9, 10, and 11. Orbital perigee was near the Ancon meridian, but ~23° to the north of the station. PLP data plotted in Figure 9 (top) show little difference between 1 s and 1 min resolution measurements. The spectrogram shows weak irregularities spread across the eastern Pacific through the South American longitude sector.

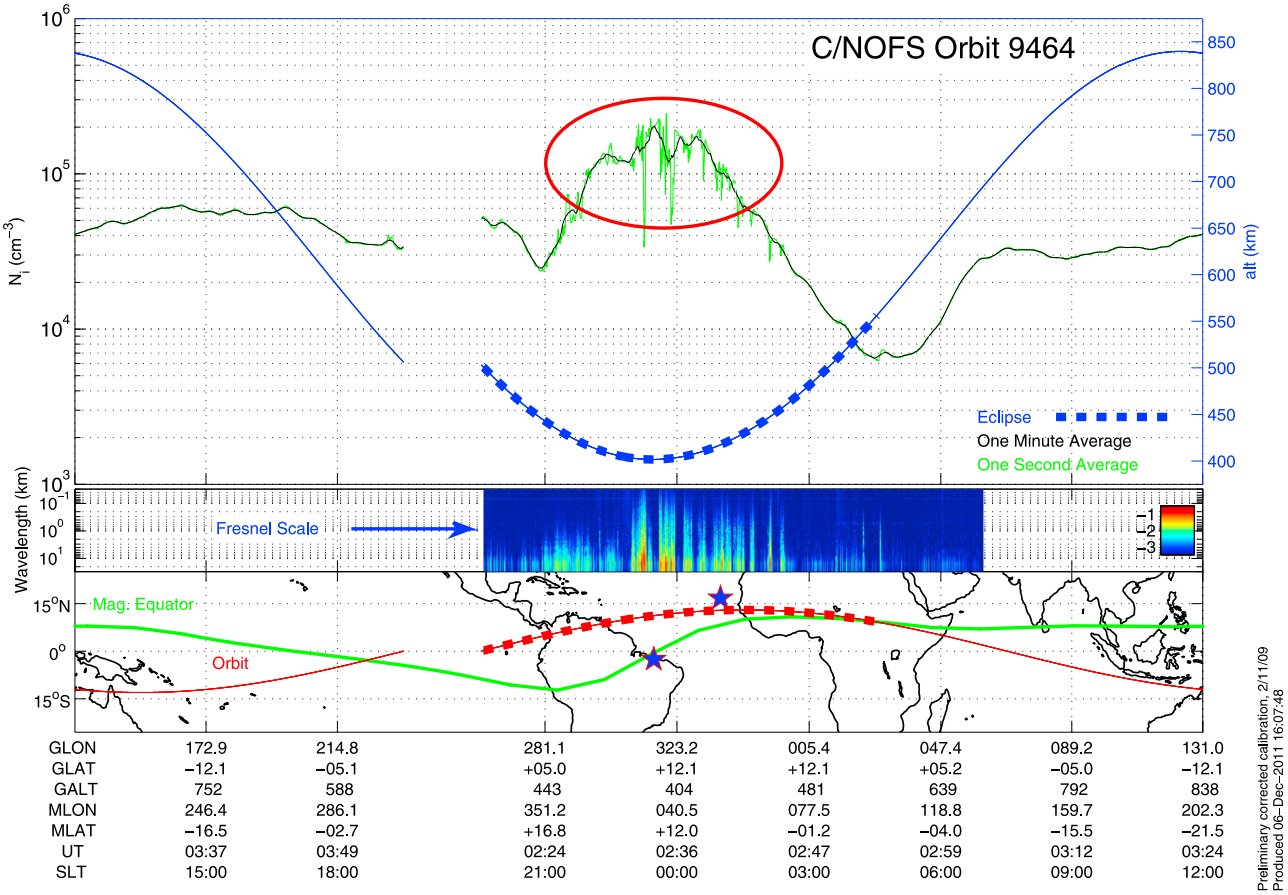

Figure 6. Plasma densities and orbital characteristics measured during C/NOFS orbit 9464, presented in the same format as Figure 2.

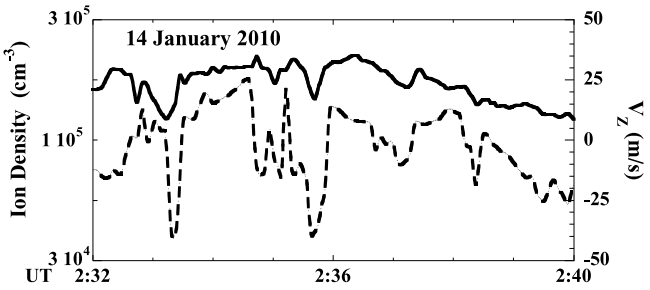

Figure 7. Ion densities (dashed line) and vertical component of drift (solid line) measured by CINDI as C/NOFS crossed a region of irregularities during orbit 9464.

Figure 1 (bottom) shows that at Ancon the S4 index had fallen from 0.6 to 0.4 at the time of orbit 9466. CINDI measurements in Figure 10 indicate that the ionosphere was generally descending, except during intervals when C/NOFS crossed density enhancements. These enhanced-density structures are very much like previously reported "plasma blobs" [*Park et al.*, 2008, and references therein]. Plasma within them was rising relative to that in nearby flux tubes. PSD calculations shown in Figure 11d indicate that within the local density enhancements significant irregularity power was present at 1 km scale sizes. The Fresnel-scale power trace in the second panel of Figure 11 shows that irregularities were more broadly spread than those found in the depletion examples in Figures 4 and 8. However, within density enhancements crossed between 05:47 and 05:49 UT, the spectral power of the kilometer-scale irregularities was a factor of 6 above an elevated background.

4. Summary and Discussion

[15] In the previous section, we examined plasma and electric fields measured by sensors on the C/NOFS satellite during an 8 h period on the UT night of 13–14 January 2010, when three SCINDA stations recorded episodes of moderate to strong (S4 $\geq$ 0.5) scintillation of 250 MHz signals. Reported satellite measurements were acquired in the evening local time sector while C/NOFS was near perigee. Throughout the period of interest, the level of geomagnetic activity was quite low. Calculations with the PBMOD ionospheric model [*Retterer et al.*, 2005] indicate that at low magnetic latitudes in the evening local time sector $h_M F_2$ ranged between 350 and 375 km. Since perigee for the C/NOFS orbit is 400 km, all satellite measurements considered here were taken at topside altitudes above the nominal peak of the *F* layer. During the reported orbits, C/NOFS encountered >100 km scale plasma density depletions/enhancements with embedded smaller-scale irregularities that extended down to at least 10 m. In all cases, the large-scale irregularities contained significant spectral power at the ~1 km Fresnel scale required to produce strong scintillations of 250 MHz signals on the ground [*Rufenach*, 1975]. Comparisons of plasma densities and vertical drifts show that the reported measurements conveniently divide

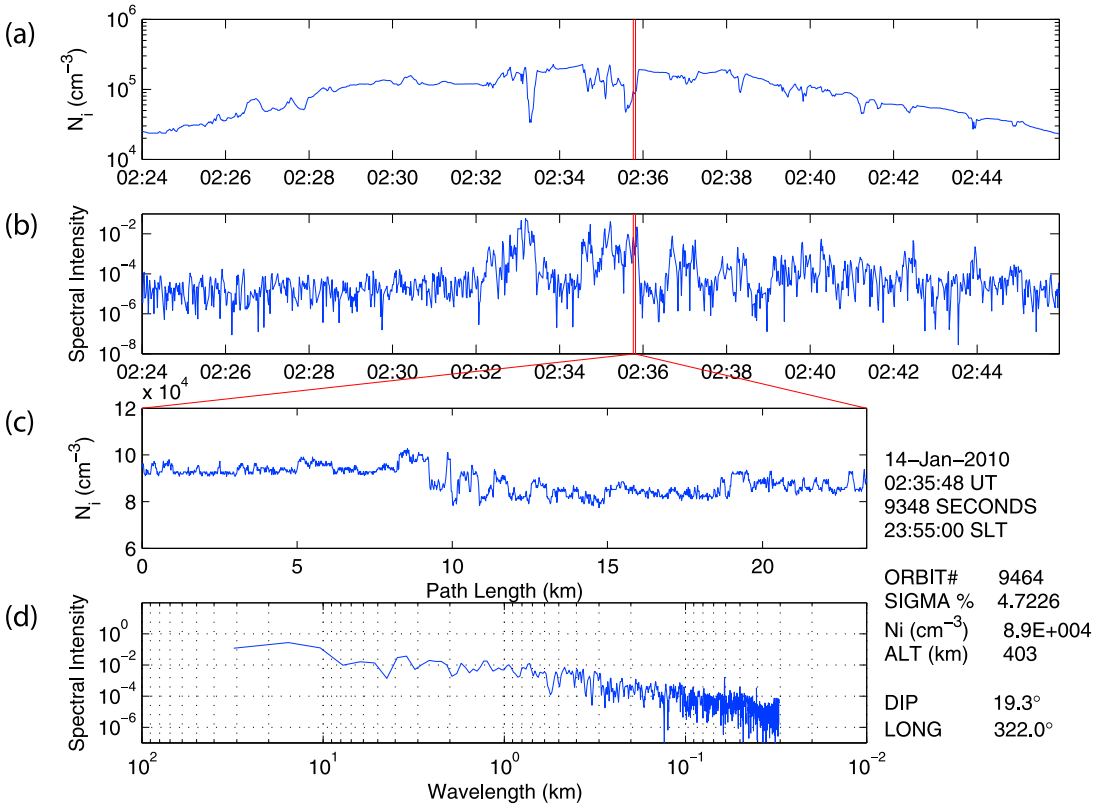

Figure 8. Plasma densities and power spectral characteristics sampled during C/NOFS orbit 9464 on 14 January 2010, presented in the same format as Figure 4.

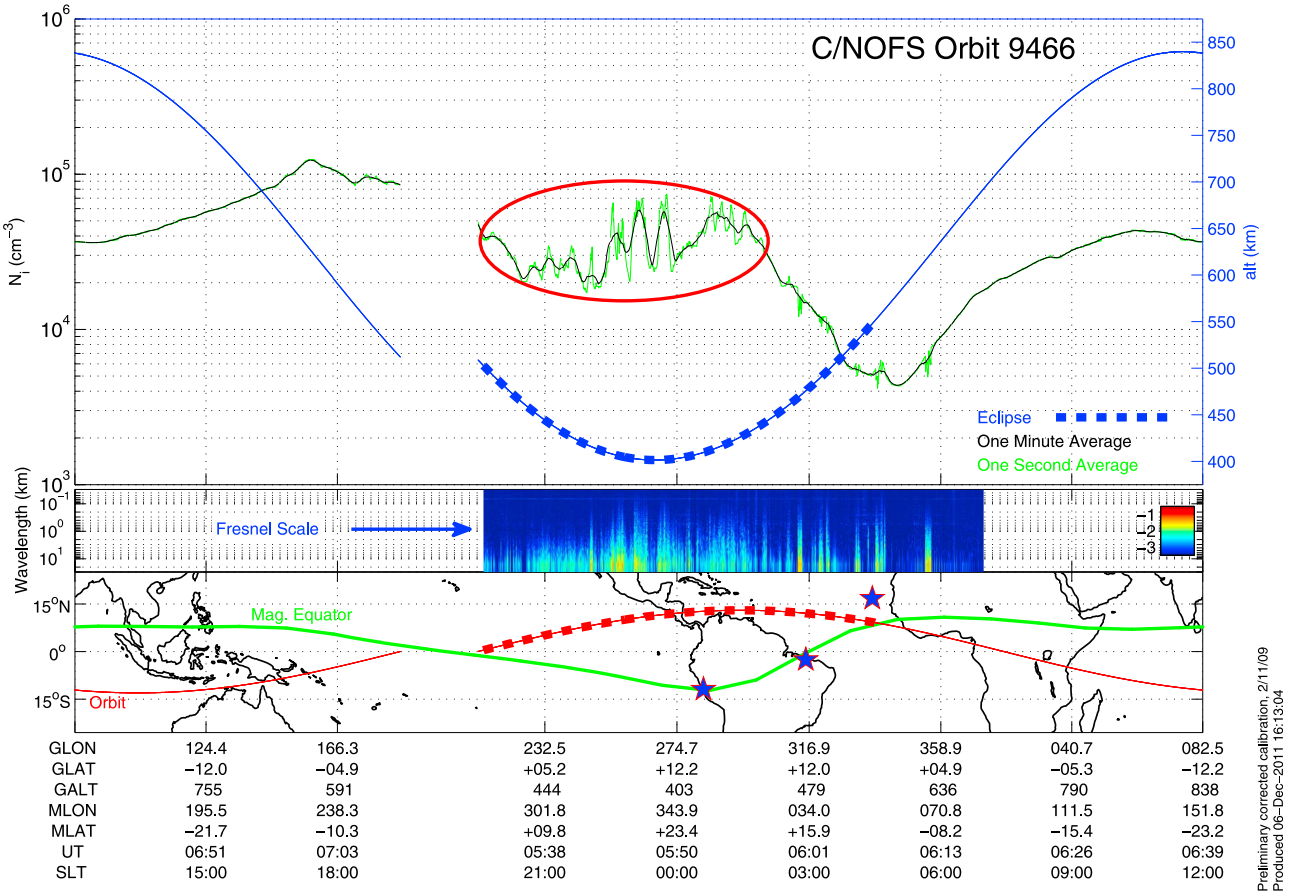

Figure 9. Plasma densities and orbital characteristics measured during C/NOFS orbit 9466 on 14 January 2010, presented in the same format as Figure 2.

into three groups: (1) depletions that drift upward, (2) depletions that drift downward relative to plasma on nearby flux tubes, and (3) enhancements that drift upward relative to plasma on nearby flux tubes. Upward drifting ~100 km scale depletions were all detected near the magnetic equator and have the characteristic of equatorial plasma bubbles that originated at bottomside altitudes [*Hanson and Sanatani*, 1973] and penetrated into the topside [*Ott*, 1978]. The other phenomena, depletions that move downward and enhancements that move upward relative to plasma on adjacent flux tubes, cannot be explained as EPBs. At the times of both observations, C/NOFS was north of the magnetic equator.

[16] The presence of Fresnel-scale irregularities at C/NOFS locations and scintillations observed at nearby ground stations suggest that the two phenomena are physically connected. The well-established connection between them is that at low magnetic latitudes the bottomside of the postsunset ionosphere is in a state of unstable equilibrium. Plasma density irregularities grow at bottomside altitudes via a generalized R-T interchange instability [*Balsley et al.*, 1972; *Scannapieco and Ossakow*, 1976]. *Haerendel* [1973]

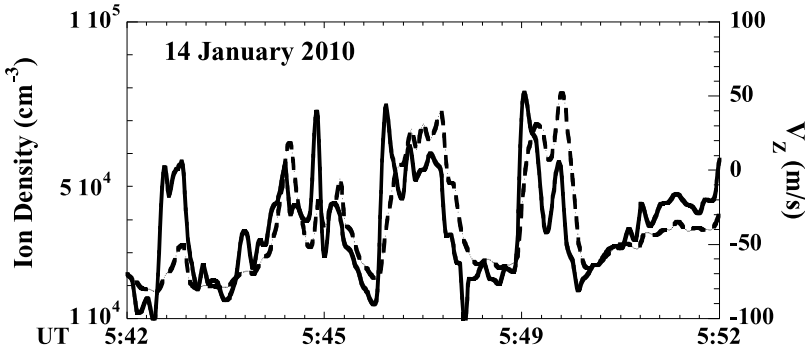

Figure 10. Ion densities (dashed line) and vertical component of drift (solid line) measured by CINDI as C/NOFS crossed a region of irregularities during orbit 9466.

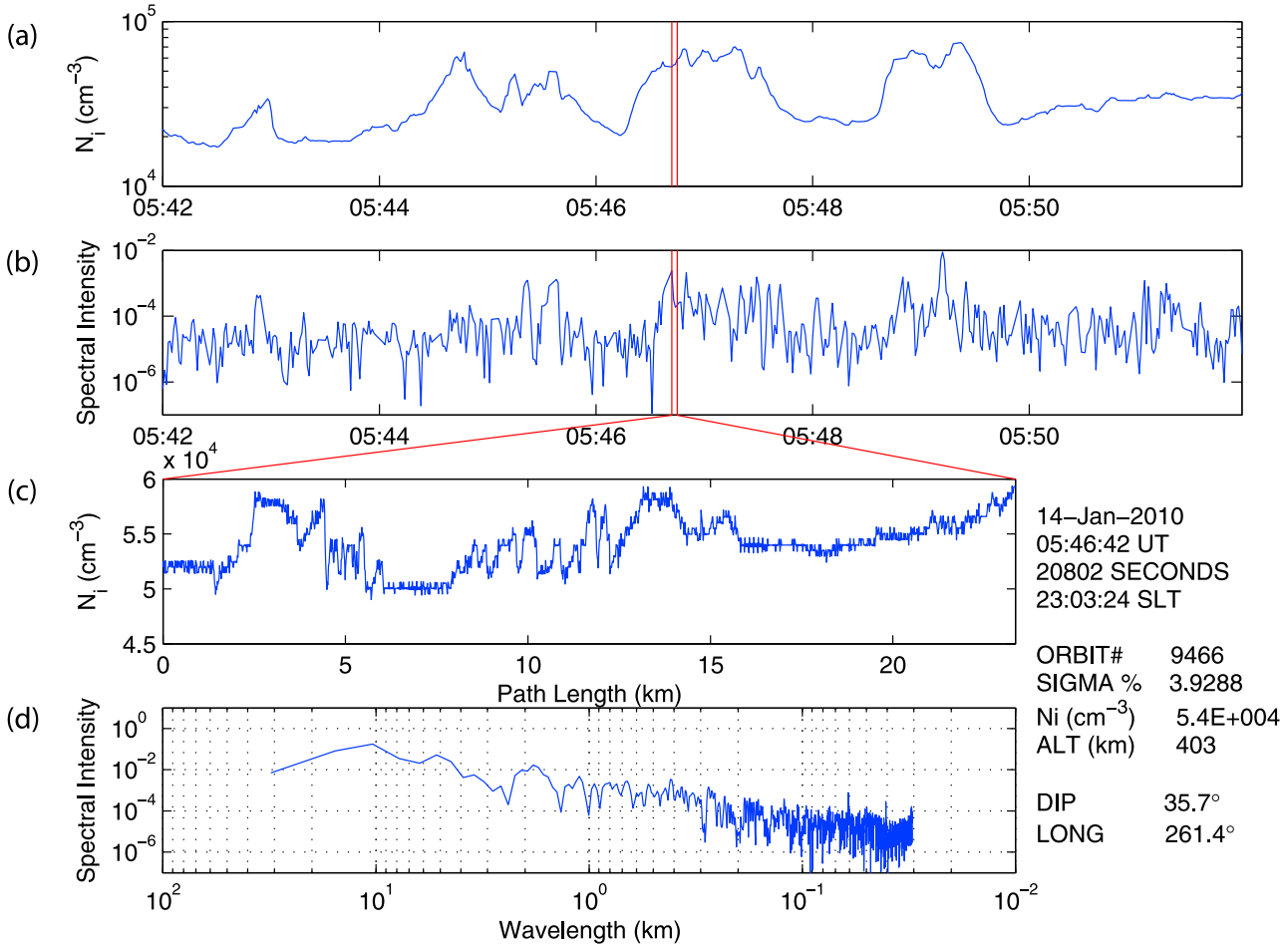

Figure 11. Plasma densities and power spectral characteristics sampled during C/NOFS orbit 9466 on 14 January 2010, presented in the same format as Figure 4.

pointed out that the R-T instability is not a purely local phenomenon. Rather, entire flux tubes are engaged. The following paragraphs indicate that these perceptions can be utilized to explain the latter two phenomena cited above. A fundamental question raised by the C/NOFS measurements is: How did information about bottomside irregularities at both large and Fresnel scales reach topside altitudes? Density gradients with respect to altitude render bottomside plasma R-T unstable and topside plasma R-T stable.

[17] Heuristically, it is useful to consider quasi-dipolar magnetic field lines that penetrate the low-latitude ionosphere at bottomside altitudes but have apex altitudes within the lower reaches of the topside ionosphere. We assume that postsunset bottomside plasma is subject to some spectrum of gravity waves from the lower atmosphere [*McClure et al.*, 1998] or a bottom-type collisional shear instability [*Hysell and Kudeki*, 2004; *Aveiro and Hysell*, 2010] that act as seeds to initiate the R-T instability. It seems highly improbable that plasma and seeding distributions at magnetically conjugate bottomside locations in the Northern and Southern Hemisphere, separated by 100 km or more, would match exactly. Rather, it seems more probable that seeding at a given time would tend to dominate in one hemisphere over the other.

[18] The diagrams in Figure 12 schematically represent two views of such a seeding event. The upper diagram provides a northward-looking, vertical cross-sectional view of the bottomside layer at the southern part of the flux tube. A sinusoidal disturbance has been introduced near the layer's lower boundary. To maintain continuity of eastward current density $\mathbf{j} = nM\ (\mathbf{g} \times \mathbf{B}_0)/B_0^2$ at the perturbed interface, a westward polarization electric field $\delta\mathbf{E}$ develops in the local density enhancement that causes the affected plasma to move downward. Here n and M represent the local plasma density and the mass of its constituent ion species, respectively. The vectors $\mathbf{g}$ and $\mathbf{B}_0$ represent the acceleration due to gravity and the local magnetic field. Conversely, eastward polarization electric fields are generated within the depleted segment causing it to rise.

[19] Although the natural phenomenon probably involves a hybrid solution [*Aveiro et al.*, 2012], it is useful to consider two artificially extreme electric field configurations: (1) Debye-like sheaths form around the polarization charges so that $\delta\mathbf{E}$ develops a strong, local component along $\mathbf{B}_0$, and (2) $\delta\mathbf{E}$ remains essentially perpendicular to $\mathbf{B}_0$. In the first case, the $\delta\mathbf{E}$ disturbance is purely local, and because of shielding no information about the bottomside disturbance propagates to topside altitudes. The second case allows the possibility that information about the changed conditions can be

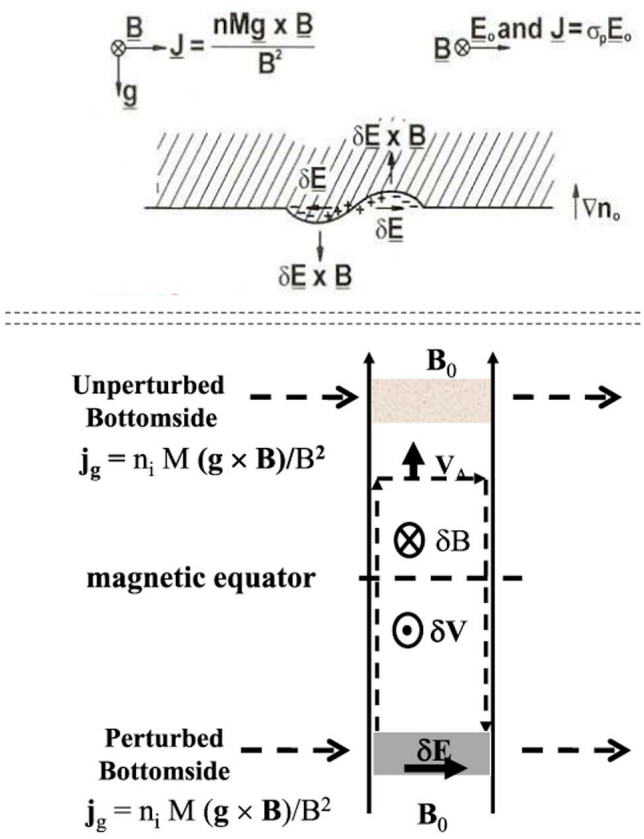

Figure 12. Two schematic views of a R-T disturbance initiated in the Southern Hemisphere intersection of a low-latitude magnetic flux tube with the bottomside ionosphere. (top) A vertical-azimuthal cross section of the bottomside ionosphere where a disturbance is initiated along its lower boundary. (bottom) View of the affected flux tube from above. An information-carrying Alfvén wave is launched from the disturbed region toward the quiescent conjugate ionosphere. Adapted from *Kelley* [2009].

reflected along the affected flux tube into the topside ionosphere. Since C/NOFS encountered multiscale density and electric field perturbations at topside altitudes where the plasma should be stable, with adjustments the second scenario is more plausible. This is the scenario postulated by *Haerendel* [1973]. The question now devolves to: "What physical mechanism is responsible for the propagation of information from a bottomside site to a topside location?"

[20] *Siscoe* [1983] showed that intermediate (Alfvén) waves are the only magnetohydrodynamic mode that is capable of carrying field-aligned currents. *Kan and Sun* [1985] demonstrated that the current density $\mathbf{j}_A$ associated with traveling Alfvén waves is

$$\mathbf{j}_A = \pm \sum_A \left[\hat{\mathbf{B}}_0 \nabla \cdot \delta\mathbf{E} + (\mathbf{B}_0 \cdot \nabla)\delta\mathbf{E} \right] \quad (1)$$

Here $\hat{\mathbf{B}}_0$ is a unit vector along the main magnetic field, $\Sigma_A = 1/\mu_0 V_A$ is the Alfvén conductance and V_A is the Alfvén speed. Figure 12 (bottom) views the affected magnetic flux tube from above. Again, only the southern bottomside layer is initially perturbed. As polarization electric fields turn on or increase, Alfvén waves are launched [*Basu*, 2005]. As indicated by equation (1), field-aligned currents propagate by laying down the space charge ($\nabla \cdot \delta\mathbf{E}$) required to maintain magnetic field lines at new equipotential levels. At the leading edges of the Alfvénic fronts, cross-field, polarization currents are carried by ions as they experience time-dependent changes in local electric fields. In the case shown in Figure 12, an Alfvénic current loop with an eastward $\delta\mathbf{E}$ produces a downward magnetic perturbation $\delta\mathbf{B}$ and upward plasma drift $\delta\mathbf{V}$.

[21] The highly idealized model pictured in Figure 12 shows a single Alfvénic disturbance. Data presented above indicate that in reality a broad spectrum of multiscale Alfvén waves may be present in evolving R-T disturbed flux tubes. The polarization electric field $\delta\mathbf{E}$ associated with the largest (~100 km) scale perturbations gives rise to upward or downward plasma motion depending on its east-west polarity. Alfvénic mapping provides a plausible mechanism for explaining CINDI detections of downward moving depletions (Figure 7) and upward moving density enhancements (Figure 10). Figure 13 represents two parcels of plasma in the topside ionosphere and their conjugate images at higher latitudes in the bottomside layer. The downward moving (yellow) parcel would be magnetically conjugate to a local density enhancement in the bottomside layer. As indicated in Figure 12 (top), the associated polarization electric field $\delta\mathbf{E}$ is westward and plasma drift $\delta\mathbf{V}$ is downward. In the topside of the *F* layer, where the density gradient is negative, downward $\delta\mathbf{V}$ carries plasma to altitudes

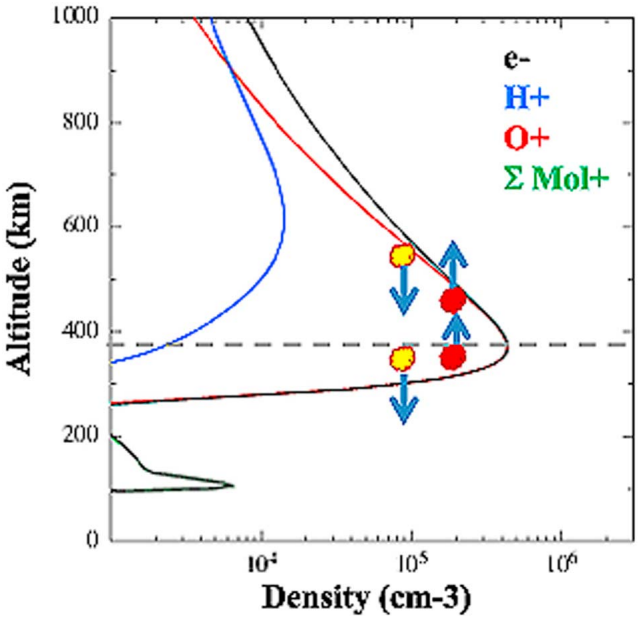

Figure 13. Schematic representation of responses of conjugate plasma parcels at topside and bottomside altitudes to an evolving Rayleigh-Taylor instability. The downward moving parcel (yellow) appears as a local enhancement at bottomside altitudes and as a local depletion in the topside. Conversely, upward moving depletions (red) at bottomside altitudes appear as enhancements in the topside.

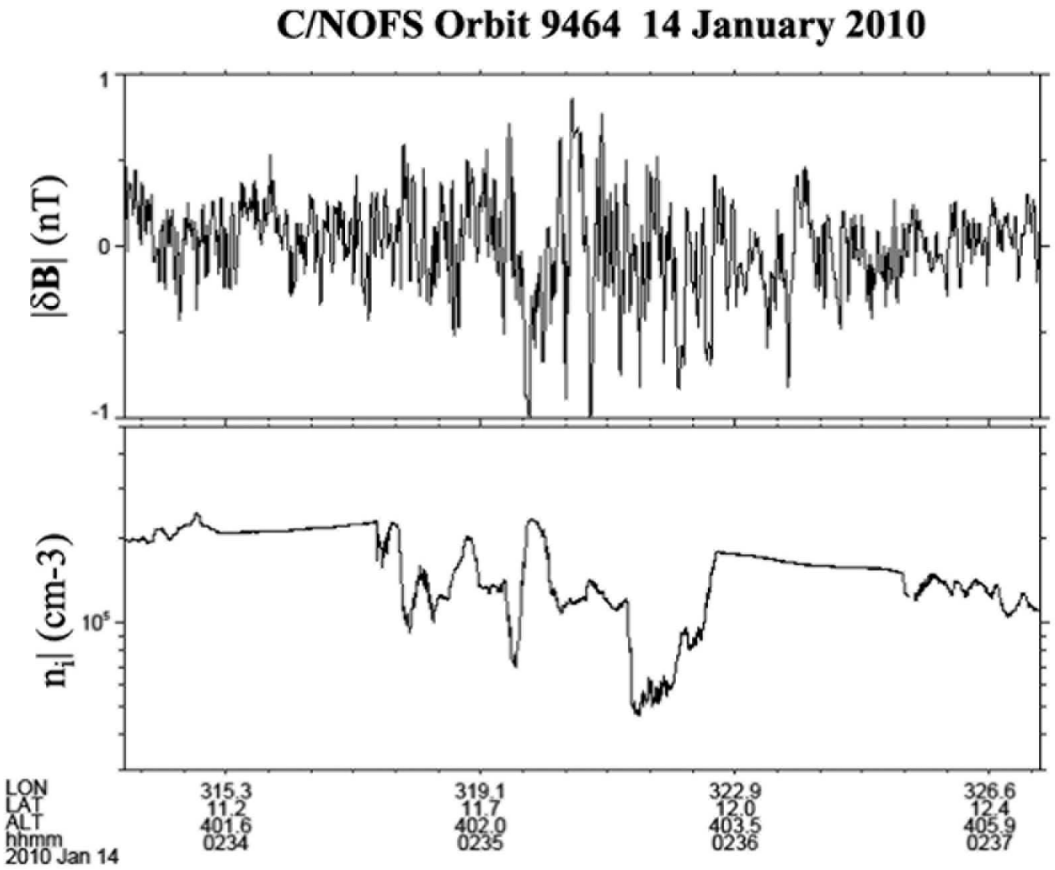

Figure 14. Example of (top) total magnetic perturbation $|\delta\mathbf{B}|$ and (bottom) ion densities, measured by VEFI during the eveningside pass of C/NOFS orbit 9464.

where it appears as a local depletion. Conversely, bottomside depletions require eastward $\delta\mathbf{E}$ and upward $\delta\mathbf{V}$. As indicated in Figure 13, mapping to the topside eastward $\delta\mathbf{E}$ causes conjugate plasma parcels (red) to move upward. A spacecraft moving through such displaced density structures at topside altitudes should sample local enhancements.

[22] Within both large-scale depletions and enhancements, the PLP and VEFI sensors on C/NOFS detected broadband spectra of density and electric field fluctuations. In all cases, significant spectral power was observed near the ~1 km Fresnel scale size. *LaBelle* [1985, Figure 3] shows that electric fields with scale sizes >0.1 km map efficiently between topside and bottomside altitudes on the nightside. If the Alfvén wave hypothesis described previously is valid, then these perturbations should be accompanied by low-frequency magnetic perturbations. Recently, *Stolle et al.* [2006] reported on magnetic field fluctuations observed by the polar-orbiting CHAMP satellite as it crossed through evening sector EPBs. They considered two possible mechanisms: diamagnetic currents and Alfvén waves. These should be regarded as distinguishable and complementary rather than mutually exclusive mechanisms. Diamagnetic currents appear at any pressure gradients in magnetized plasmas. Associated magnetic perturbations $\delta\mathbf{B}$ should be parallel to the main field $\mathbf{B}_0$ in depletions and antiparallel to it in enhancements. The $\delta\mathbf{B}$ associated with Alfvén waves is perpendicular to $\mathbf{B}_0$. *Stolle et al.* [2006] investigated the Poynting fluxes associated with $\delta\mathbf{B}$ perturbations and compared them with predictions of a transmission line model with the generator near the field line apex as proposed by *Bhattacharyya and Burke* [2000]. While inferred Poynting fluxes sometimes appeared to come from the equator, they often propagated from the lower ionosphere toward the equatorial field-line apex. This result is consistent with predictions of the simple model illustrated in Figure 12.

[23] A detailed discussion on the electromagnetic nature of information flow between the bottomside and topside of the ionosphere exceeds the scope of this report. Still, the question remains: Is there any empirical evidence for the presence of small-scale $\delta\mathbf{B}$ structures embedded within ~100 km topside enhancements/depletions? Data plotted in Figure 14 provide a partial answer. Figure 14 (top) shows the total magnetic perturbation $\delta\mathbf{B}$ measured between 02:33:30 and 02:37:30 UT on 14 January 2010. The trace in Figure 14 (bottom) shows ion densities. Clear evidence of low-frequency $\delta\mathbf{B}$ variations is present in the data streams. Consistent with the Alfvén wave hypothesis, the amplitudes of magnetic perturbations observed between 02:34 and 02:36 UT were mostly directed perpendicular to the main field ($\delta\mathbf{B}_{\|} \ll \delta\mathbf{B}_{\perp}$). Peak-to-peak amplitudes ≥1 nT are apparent in the vicinity of the large depletions that C/NOFS crossed. However, in the surrounding smooth-density intervals, magnetic oscillations of somewhat weaker amplitudes were also observed. At the present level of analysis, we

regard the magnetic field evidence as suggestive but not compelling. Note that observed perturbations represent superpositions of initial and reflected $\delta\mathbf{E}$ and $\delta\mathbf{B}$ waves, with travel times between magnetic conjugate points at low latitudes of <1 s. Thus, the ratios of the superposed amplitudes do not match the local Alfvén speed. It is also presently difficult to determine the rate or even the direction of electromagnetic energy flow. The fast reflection time indicates that the electrostatic approximation that assumes information travels at the speed of light is adequate for quantitative modeling of the growth of the R-T instability.

5. Conclusion

[24] In this paper we have analyzed plasma and field measurements acquired by the C/NOFS satellite during an 8 hour period on 13–14 January 2010 when 250 MHz scintillation activity was observed at nearby SCINDA ground stations. In our three examples, C/NOFS detected relatively small-scale density and electric field irregularities embedded within large-scale (∼100 km) structures at topside altitudes. The fact that significant spectral power was measured at the Fresnel-scale (∼1 km) size suggests that C/NOFS was magnetically conjugate to bottomside irregularities similar to those directly responsible for the observed scintillations. Ion drift meter plasma density measurements indicate three distinct types of large-scale irregularities, namely, upward moving depletions, downward moving depletions, and upward moving density enhancements. While the first type bears the characteristics of equatorial plasma bubbles, the second and third do not. We have suggested a simple model that regards small-scale irregularities at topside altitudes as Alfvénic images of bottomside irregularities. While examples of upward-directed Poynting fluxes measured by the CHAMP satellite in the low-latitude ionosphere are consistent with this interpretation [*Stolle et al.*, 2006], the presented C/NOFS evidence can, at this point, only be regarded as suggestive.

[25] **Acknowledgments.** Support for the present work was provided by the Air Force Office of Scientific Research, Task 12RV10COR, and AF contract FA8718-08-C-0012 with Boston College. The authors are very grateful to R. A. Heelis for helpful discussions about the possible roles of Alfvén waves in the development of the Rayleigh-Taylor instability.

[26] Robert Lysak thanks the reviewers for their assistance in evaluating this paper.

References

Aggson, T. L., W. J. Burke, N. C. Maynard, W. B. Hanson, W. R. Hogey, J. L. Saba, and J. A. Slavin (1992), Equatorial bubbles updrafting at supersonic speeds, *J. Geophys. Res.*, *97*, 8581–8590, doi:10.1029/92JA00644.

Aveiro, H. C., and D. L. Hysell (2010), Three-dimensional numerical simulation of equatorial *F* region plasma irregularities with bottomside shear flow, *J. Geophys. Res.*, *115*, A11321, doi:10.1029/2010JA015602.

Aveiro, H. C., D. L. Hysell, R. Caton, K. Groves, J. Klenzing, R. F. Pfaff, R. Stoneback, and R. A. Heelis (2012), Three-dimensional numerical simulations of equatorial spread F: Results and observation in the Pacific sector, *J. Geophys. Res.*, doi:10.1029/2011JA017077, in press.

Balsley, B., G. Haerendel, and R. Greenwald (1972), Equatorial spread F: Recent observations and a new interpretation, *J. Geophys. Res.*, *77*, 5625–5628, doi:10.1029/JA077i028p05625.

Basu, B. (2005), Characteristics of electromagnetic Rayleigh-Taylor modes in nighttime equatorial plasma, *J. Geophys. Res.*, *110*, A02303, doi:10.1029/2004JA010659.

Bhattacharyya, A., and W. J. Burke (2000), A transmission line analogy for the development of equatorial plasma bubbles, *J. Geophys. Res.*, *105*, 24,941–24,950, doi:10.1029/1999JA000458.

Burke, W. J., C. Y. Huang, C. E. Valladares, J. S. Machuzak, L. C. Gentile, and P. J. Sultan (2003), Multipoint observations of equatorial plasma bubbles, *J. Geophys. Res.*, *108*(A5), 1221, doi:10.1029/2002JA009382.

Burke, W. J., O. de La Beaujardière, L. C. Gentile, D. E. Hunton, R. F. Pfaff, P. A. Roddy, Y.-J. Su, and G. R. Wilson (2009), C/NOFS observations of plasma density and electric field irregularities at postmidnight local times, *Geophys. Res. Lett.*, *36*, L00C09, doi:10.1029/2009GL038879.

de La Beaujardière, O., et al. (2004), C/NOFS: A mission to forecast scintillation, *J. Atmos. Sol. Terr. Phys.*, *66*, 1573–1591, doi:10.1016/j.jastp.2004.07.030.

de La Beaujardière, O., P. A. Roddy, Y.-J. Su, J. M. Retterer, G. R. Wilson, W. J. Burke, L. C. Gentile, D. E. Hunton, and D. L. Cooke (2009), C/NOFS observations of deep plasma depletions at dawn, *Geophys. Res. Lett.*, *36*, L00C06, doi:10.1029/2009GL038884.

Farley, D., E. Bonelli, B. Fejer, and M. Larsen (1986), The prereversal enhancement of the zonal electric field in the equatorial ionosphere, *J. Geophys. Res.*, *91*, 13,723–13,728, doi:10.1029/JA091iA12p13723.

Fejer, B. G., and L. Scherliess (1995), Time dependent response of equatorial ionospheric electric fields to magnetospheric disturbances, *Geophys. Res. Lett.*, *22*, 851–854, doi:10.1029/95GL00390.

Gentile, L. C., W. J. Burke, and F. J. Rich (2006), A climatology of equatorial plasma bubbles from DMSP 1989–2004, *Radio Sci.*, *41*, RS5S21, doi:10.1029/2005RS003340.

Gentile, L. C., W. J. Burke, P. A. Roddy, J. M. Retterer, and R. T. Tsunoda (2011), Climatology of plasma density depletions observed by DMSP in the dawn sector, *J. Geophys. Res.*, *116*, A03321, doi:10.1029/2010JA016176.

Groves, K. M., et al. (1997), Equatorial scintillation and systems support, *Radio Sci.*, *32*, 2047–2064, doi:10.1029/97RS00836.

Haerendel, G. (1973), *Theory of Equatorial Spread F*, report, Max-Planck Inst. für Extraterr. Phys., Garching, Germany.

Hanson, W. B., and S. Sanatani (1973), Large Ni gradients below the equatorial *F*-peak, *J. Geophys. Res.*, *78*, 1167–1173, doi:10.1029/JA078i007p01167.

Huang, C. Y., W. J. Burke, J. S. Machuzak, L. C. Gentile, and P. J. Sultan (2001), DMSP observations of equatorial plasma bubbles in the topside ionosphere near solar maximum, *J. Geophys. Res.*, *106*, 8131–8142, doi:10.1029/2000JA000319.

Huang, C. Y., W. J. Burke, J. S. Machuzak, L. C. Gentile, and P. J. Sultan (2002), Equatorial plasma bubbles observed by DMSP satellites during a full solar cycle: Toward a global climatology, *J. Geophys. Res.*, *107*(A12), 1434, doi:10.1029/2002JA009452.

Hysell, D. L., and E. Kudeki (2004), Collisional shear instability in the equatorial *F* region ionosphere, *J. Geophys. Res.*, *109*, A11301, doi:10.1029/2004JA010636.

Kan, J. R., and W. Sun (1985), Simulation of the westward travelling surge and Pi 2 pulsations during substorms, *J. Geophys. Res.*, *90*, 10,911–10,923, doi:10.1029/JA090iA11p10911.

Kelley, M. C. (2009), *The Earth's Ionosphere: Plasma Physics and Electrodynamics*, Academic, Elsevier, London.

LaBelle, J. (1985), Mapping of electric field structures from the equatorial *F* region to the underlying *E* region, *J. Geophys. Res.*, *90*, 4341–4346, doi:10.1029/JA090iA05p04341.

McClure, J. P., S. Singh, B. K. Bamgboye, F. S. Johnson, and H. Kil (1998), Occurrence of equatorial *F* region irregularities: Evidence for tropospheric seeding, *J. Geophys. Res.*, *103*, 29,119–29,135, doi:10.1029/98JA02749.

Ott, E. (1978), Theory of Rayleigh-Taylor bubbles in the equatorial ionosphere, *J. Geophys. Res.*, *83*, 2066–2070, doi:10.1029/JA083iA05p02066.

Park, J., C. Stolle, H. Lühr, M. Rother, S.-Y. Su, W. W. Min, and J.-J. Lee (2008), Magnetic signatures and conjugate features of low latitude plasma blobs as observed by the CHAMP satellite, *J. Geophys. Res.*, *113*, A09313, doi:10.1029/2008JA013211.

Pfaff, R., et al. (2010), Observations of DC electric fields in the low latitude ionosphere and their variations with local time, longitude, and plasma density during extreme solar minimum, *J. Geophys. Res.*, *115*, A12324, doi:10.1029/2010JA016023.

Pottelette, R., M. Malingre, J. J. Berthelier, E. Seran, and M. Parrot (2007), Filamentary Alfvénic structures excited at the edges of equatorial plasma bubbles, *Ann. Geophys.*, *25*, 2159–2165, doi:10.5194/angeo-25-2159-2007.

Retterer, J. M., D. T. Decker, W. S. Borer, R. E. Daniell, and B. G. Fejer (2005), Assimilative modeling of the equatorial ionosphere for scintillation forecasting: Modeling with vertical drifts, *J. Geophys. Res.*, *110*, A11307, doi:10.1029/2002JA009613.

Roddy, P. A., D. E. Hunton, J. O. Ballenthin, and K. M. Groves (2010), Correlation of in situ measurements of plasma irregularities with

ground-based scintillation observations, *J. Geophys. Res.*, *115*, A06303, doi:10.1029/2010JA015288.

Rufenach, C. L. (1975), Ionospheric scintillation by a random phase screen: Spectral approach, *Radio Sci.*, *10*, 155–165, doi:10.1029/RS010i002p00155.

Scannapieco, A. J., and S. L. Ossakow (1976), Nonlinear equatorial spread *F*, *Geophys. Res. Lett.*, *3*, 451–454, doi:10.1029/GL003i008p00451.

Siscoe, G. L. (1983), Solar system magnetohydrodynamics, in *Solar Terrestrial Physics*, edited by R. L. Carovillano and J. M. Forbes, pp. 11–100, D. Reidel, Dordrecht, Netherlands.

Stolle, C., H. Lühr, M. Rother, and G. Balasis (2006), Magnetic signatures of equatorial spread *F* as observed by the CHAMP satellite, *J. Geophys. Res.*, *111*, A02304, doi:10.1029/2005JA011184.

W. J. Burke, L. C. Gentile, P. A. Roddy, and S. R. Shomo, Air Force Research Laboratory Space Vehicles Directorate, 29 Randolph Rd., Hanscom AFB, MA 01731, USA. (afrl.rvborgmailbox@kirtland.af.mil)

R. F. Pfaff, NASA Goddard Space Flight Center, Mail Code 674, Greenbelt, MD 20771, USA.